Cell Reports
Physical Science

CellPress
OPEN ACCESS

Article

Increasing generalization capability of battery health estimation using continual learning

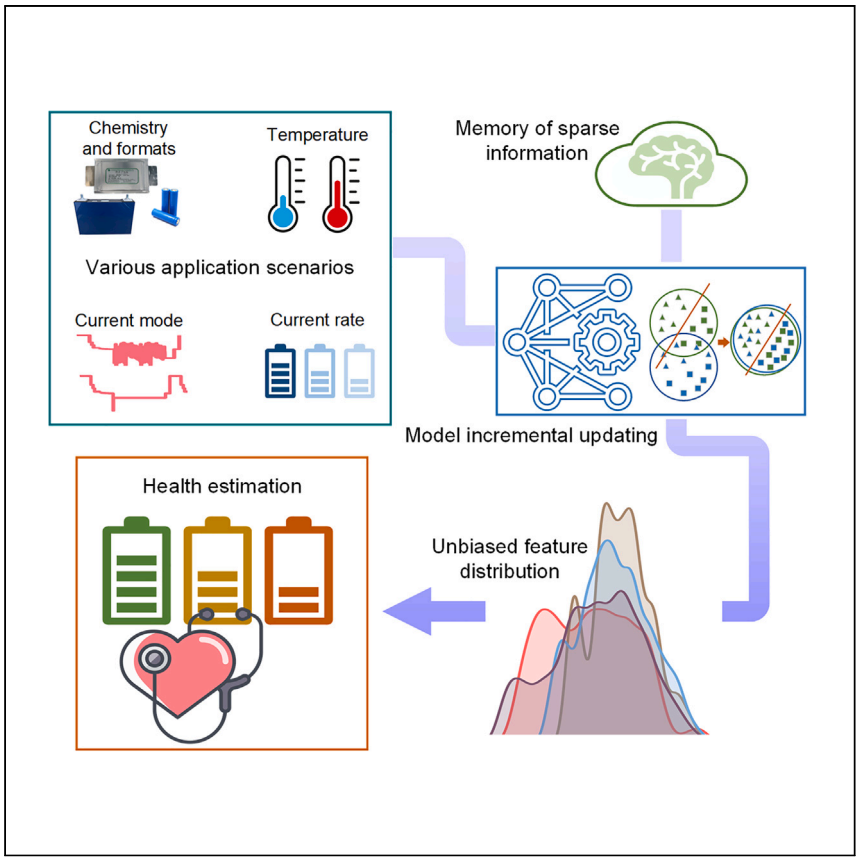

Che et al. demonstrate the approach and significance of using domain adaptative continual learning to incrementally increase the generalization ability of battery health estimation model. The model ensures estimations under various scenarios related to practical applications for different batteries in their different lifetimes, with interpretations of unbiased feature distributions and avoidance of catastrophic forgetting.

Yunhong Che, Yusheng Zheng, Simona Onori, Xiaosong Hu, Remus Teodorescu

sonori@stanford.edu (S.O.)
xiaosonghu@ieee.org (X.H.)

Highlights

Improving model generalization incrementally for battery health estimation

Applicable under various working conditions without catastrophic forgetting

Model is interpretable with unbiased feature distributions

Generate large aging datasets for prismatic and pouch batteries

Che et al., Cell Reports Physical Science 4, 101743
December 20, 2023
https://doi.org/10.1016/j.xcrp.2023.101743

Cell Reports
Physical Science

CellPress
OPEN ACCESS

Article

Increasing generalization capability of battery health estimation using continual learning

Yunhong Che,[1,2] Yusheng Zheng,[1,4] Simona Onori,[2,*] Xiaosong Hu,[3,5,*] and Remus Teodorescu[1]

SUMMARY

Accurate and reliable estimation of battery health is crucial for predictive health management. We report a strategy to strengthen the accuracy and generalization of battery health estimation. The model can be initially built based on one battery and then continuously updated using unlabeled data and sparse limited labeled data collected in early stages of testing batteries in different scenarios, satisfying incremental improvement in practical applications. We generate our datasets from 55 commercial pouch and prismatic batteries aged for more than 116,000 cycles under various scenarios. Our model achieves a root mean-square error of 1.312% for the estimation of different dynamic current modes and rates and variable temperature conditions over the entire lifespan using partial charging data. Our model is interpreted by the post hoc strategy with unbiased hidden features, prevents catastrophic forgetting, and supports estimation using data collected in 3 min during ultra-fast charging with errors of less than 2.8%.

INTRODUCTION

Lithium-ion batteries occupy main roles in energy storage systems for electric vehicles, portable electronics, smart grids, and other electrified devices.[1,2] However, battery degradation is unavoidable during storage and usage due to numerous aging-related side reactions that occur during charging, discharging, and storage, resulting in irreversible capacity and power decades.[3–5] State of health (SOH), which is generally defined as a ratio of current capacity to the initial capacity, is one key indicator to represent the health state of batteries.[6,7] It helps release the anxiety of cruise concern, fear of failure, and over-usage from consumers, and guides proper maintenance and retirement for second-life applications.[8–10] Therefore, one critical and urgent challenge that must be addressed is indirect and accurate SOH estimation for commercial lithium-ion batteries.

A wealth of literature has been published on this topic. Model-based approaches aim to build physical models for the characterization of the microscopic electrochemical reactions, including the growth of solid electrolyte interphase films, loss of active material, cathode oxidation, lithium plating, etc.,[11–13] to estimate the health of batteries through the estimation of aging-related parameters. The physical interpretation of the parameters is the most advantageous aspect, whereas the high computational burden and complex solving work prevent the practical deployment in a battery management system.[14] As a result, recent research focuses more on data-driven methods for battery health prognostics, which benefit from good flexibility, transferability, extrapolation capability, etc.

The general idea behind the data-driven methods is to use machine learning models to directly map the relationship between the available parameters/features and the

[1]Department of Energy, Aalborg University, 9220 Aalborg, Denmark

[2]Department of Energy Science and Engineering, Stanford University, Stanford, CA 94305, USA

[3]College of Mechanical and Vehicle Engineering, Chongqing University, Chongqing 400044, China

[4]Department of Mechanical Engineering, Imperial College London, London SW7 2AZ, UK

[5]Lead contact

*Correspondence: sonori@stanford.edu (S.O.), xiaosonghu@ieee.org (X.H.)

https://doi.org/10.1016/j.xcrp.2023.101743

SOH.[15–17] Zhang et al.,[18] Gasper et al.,[19] and Jones et al.[20] investigated the physical relationship between the electrochemical impedance spectroscopy (EIS) curve and battery aging and used machine learning to achieve accurate estimations of battery SOH. However, acquiring EIS data online necessitates the use of specialized measurement equipment, which is costly and difficult to implement onboard. The information extracted from online measured data can also meet the requirement for battery health estimation. Zhu et al.[21] investigated the voltage relaxation after fully charging to extract several features. Previous works[22–24] have also found high correlations between the capacities and the information extracted from the discharge curve. However, the long time required for the voltage relaxation followed by the full charging and the random discharging profiles due to the load and environment in the real world presents challenges for rapid and effective estimations. The charging procedure, on the other hand, is more predictable and controllable throughout the life cycle. Information from charging curves is widely extracted for battery health estimation.[9,25–28] For example, Roman et al.[17] extracted several features from the voltage and current curves during the charging process. In practical applications, batteries are generally undergoing partial charging and partial discharging. Features extracted from partial charging curves are becoming hot topics to make the machine learning-based battery health estimation methods more robust and practical.[25,29,30] In feature-free deep learning, partial charging curves also become the research objectives. Tian and co-workers[31,32] used partial constant current curves and short pulse curves to achieve accurate and reliable EIS prediction for batteries over their entire their lifetime via deep learning. Therefore, the estimation effectiveness needs evaluation under different and shallow charging stages to verify the generalization regarding practical applications when developing the battery health prognostics methods.

Regarding the machine learning models, various algorithms have been used such as linear/multi-linear regression (LR),[33,34] Gaussian process regression (GPR),[27,28,35] support vector regression (SVR),[22,36] XGboost regression,[20,21] artificial neural networks,[37–39] etc. Although it has been demonstrated that these algorithms achieve accurate estimations, conventional data-driven models struggle to handle estimations in a variety of scenarios because of domain discrepancies existing between different batteries. Transfer learning is a promising method for improving estimation performance on testing batteries by leveraging knowledge from source batteries. It has been summarized in Liu et al.[40] that transfer learning has promoted the development of smarter battery management in modeling, state estimation, and aging prognostics, especially in recent years. Both the domain adaptation[41–43] and model parameter fine-tuning strategies[23,24,44–47] have been proven to have satisfactory performance. However, the available data from the tested batteries are most unlabeled while only very limited data can be recorded in practical industrial applications.[48,49] Conventional machine learning methods mostly ignore the effectiveness of taking advantage of unlabeled data for model improvement. Recent works[50,51] have proven that, by leveraging the information from the unlabeled data, the accuracy of the target tasks, i.e., battery SOH estimation, can be improved by either reducing the feature domain discrepancies or setting up a pre-trained model. This is significant for industrial applications since most available data are unlabeled. Therefore, the optimal use of both unlabeled data and sparsely labeled data from batteries to incrementally improve the model accuracy and generalization is worth investigating to promote industrial implementations. Conventional machine learning-based methods suffer from catastrophic forgetting,[52,53] which means that, after transfer learning, the performance of the data-driven model on the target domain improves while the estimation on source domains degrades. For the battery

health model, the model generalization on the different working conditions becomes one of the most concerned issues but such a problem cannot be tackled properly by simply updating the model using newly obtained information. The capability to estimate battery health under different scenarios with only one model is lacking. Continual learning or lifelong learning, which focuses on learning sequentially as biological systems do and maintaining the ability learned before, provides great opportunities in battery health prognostics.[54,55] The memory-based framework is easy to understand and implement while the important information that represents the learned characteristics needs investigating to alleviate the storage challenge. Poor interpretability is another major disadvantage of conventional machine learning-based methods. The interpretability of machine learning is valuable to help understand models by explaining or presenting their behaviors in some understandable terms.[56] A good explanation will improve the trust of users to adopt the machine learning model and help researchers to know why the system fails and seek safety improvement. Generally, methods for machine learning interpretability can be divided into model based and post hoc based.[57] Regarding machine learning for battery health prognostics, the model-based method can be realized by analyzing the dependencies between the physical features and the output battery health metrics.[58] It helps understand the mechanisms better while physical modeling and feature extraction are required. For the post-hoc-based method, it is significant to analyze the learned characteristics of machine learning to help interpret and understand the reason for the model behaviors, which can be applied for pure data-driven methods but is still ignored by most existing works.

In this work, we seek to investigate the way to make full use of both unlabeled data and labeled data from batteries operating under various unseen conditions to improve the accuracy and generalization of the data-driven battery health estimation models without catastrophic forgetting. Instead of using large amounts of source data for model training, we first built an initial machine learning model using data from a commonly aged battery and then improved it during different applications, making it continuously learn the aging information that covers various scenarios to satisfy the estimations under various scenarios. Only unlabeled data and limited sparsely labeled data are required for memory-based continual learning updating. As shown in Figure 1, the unlabeled data, which can be obtained from each operating cycle, are used for the unsupervised domain adaptation, while the sparsely labeled data from the testing battery (limited in practical applications) and the stored sparse data from previous scenarios are adopted for continual updating. The detailed framework introduction and model updating process are described in Note S1, methods, and Note S4. The machine learning model can be interpreted based on the unbiased hidden state distributions under different scenarios. The comparisons between existing methods are provided to explain the advantage of the proposed method regarding the performance metrics and learned characteristics interpretation. The generalization of our model is also evaluated using shallow charging processes for the different practical requirements in different implementation scenarios. Comprehensive aging datasets covering different battery chemistries, formats (pouch and prismatic), different environmental conditions, and different current modes and types are generated to verify the generalization of the proposed method under different application scenarios.

RESULTS

Data generation

Experimental data on different kinds of commercial battery cells are generated in this study. The batteries are cycled in the thermal chamber or room environment

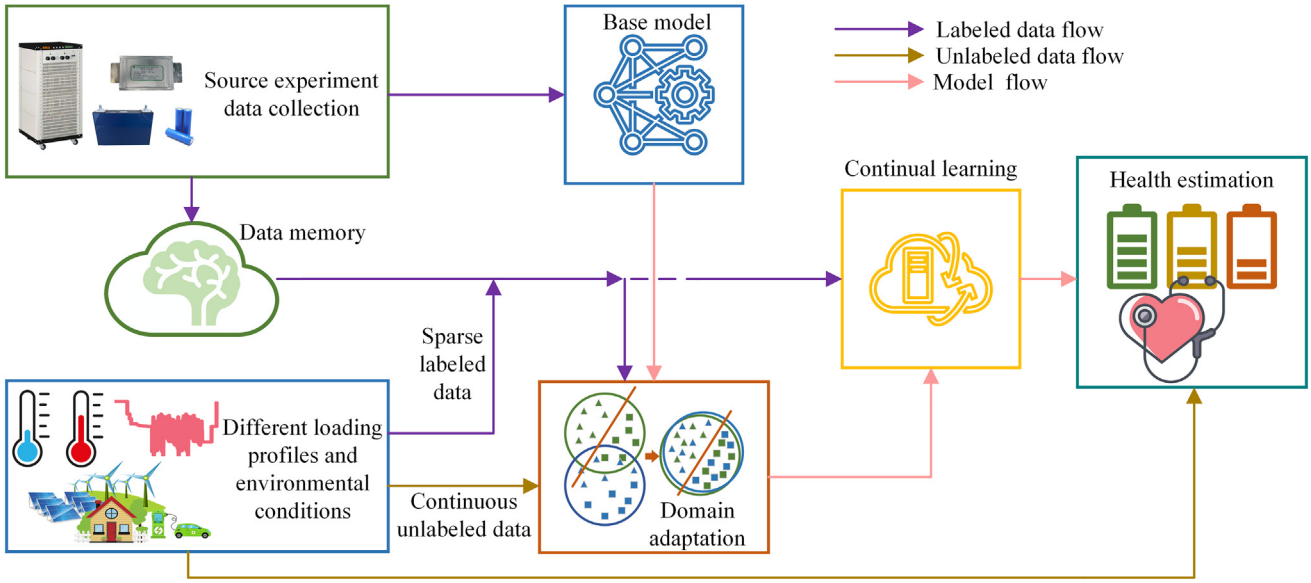

Figure 1. Workflow

The basic experiment is first conducted to collect data on one commonly aged battery. Then, the collected data is used for base model training and some spare labeled data containing full aging information is stored for later training. When the data from batteries tested with different operating profiles and environmental conditions are collected, the continuous unlabeled data, along with the stored sparsely labeled data from the source domain, is used to retrain the base model with the domain adaptation strategy. When discontinuous labeled data from the tested battery are obtained, the model is further trained on top of the domain-adapted model. Finally, online estimations are performed using the updated model.

with different current profiles and rates using the platform shown in Figure S1. These batteries are from different formats and chemistry and are aged under primary application scenarios and secondary application scenarios. The summary of the generated dataset is listed in Table S1. The detailed experimental procedure to generate these datasets is listed in Table S2 and Note S2. Different from most of the datasets in the published works,[2,18,20,21,33,48] where the small cylindrical or coin batteries were used for cycling, this paper focuses on the data generation based on pouch cells and prismatic cells. These two types of batteries are widely used in energy storage systems (e.g., EVs and grid stations), where limited source data are available at the current time. In addition, we also test batteries using dynamic discharging profiles and under variable temperatures and continue aging some of them in their secondary lifespan to make our dataset cover more aging scenarios and applications. The dynamic loadings and variable temperature conditions help emulate battery aging under practical usage with seasonal variations,[59,60] which cause the degradation curves in Figures 2B and 2C to fluctuate with the variation of environmental temperatures. A total of 55 pouch and prismatic batteries were tested with 116,681 cycles in total, which are publicly available to be used for further research on battery health prognostics. The considered information in the cycling test is shown in Figure 2A. The degradation curves of batteries in dataset 1 to dataset 5 are shown in Figures 2B–2F.

Health estimation

We first demonstrate the effectiveness of the estimations for the batteries working under different dynamic profiles and variable temperatures. The SOH is outputted by the machine learning model by inputting the partial charging capacity-voltage (Q-V) sequence. The detailed model construction and training are described in methods and Notes S1–S4. This application scenario is close to practical

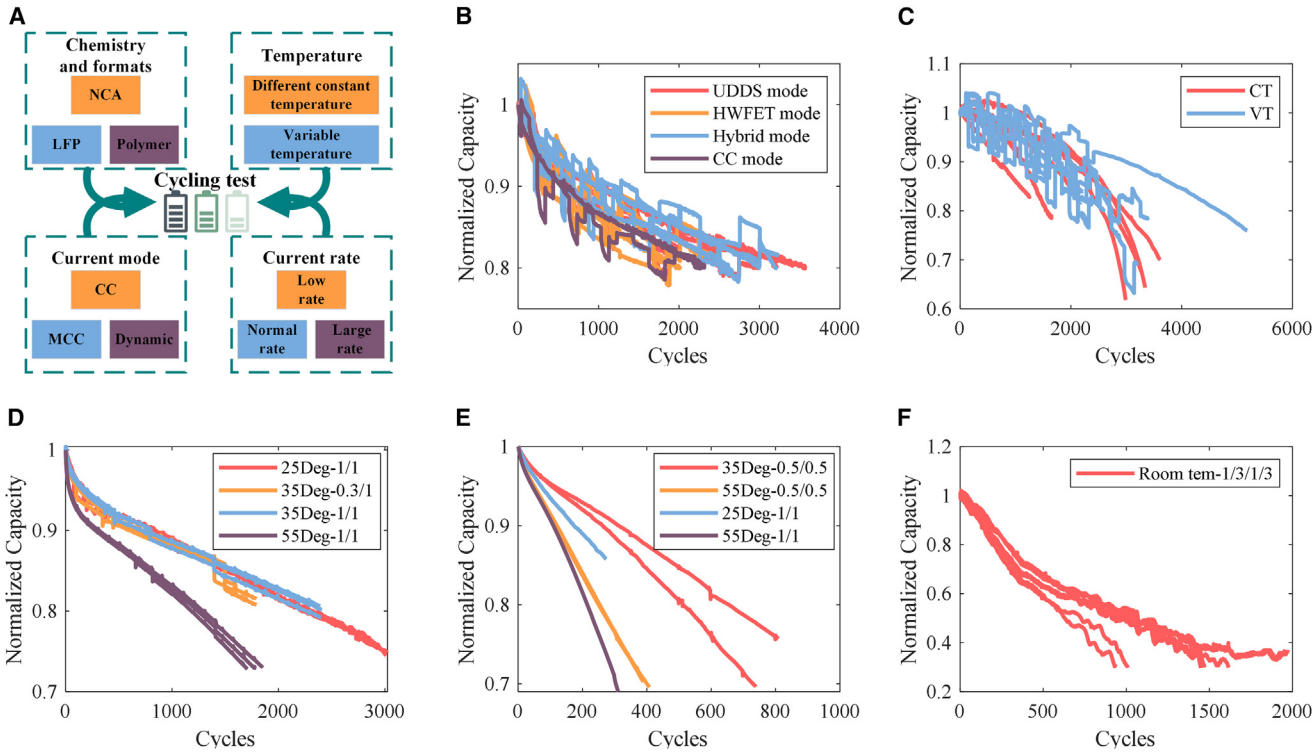

Figure 2. Cycling test for data generation and normalized capacity curves of the tested batteries

(A) The main influence factors affecting battery health estimation that are considered in the aging test, where different battery chemistry and formats, different temperature conditions, and different current modes and rates are included in the generated dataset.

(B) The normalized capacities versus aging cycles in dataset 1 with different discharging profiles and variable temperatures (cause the degradation trajectories to fluctuate with temperature variations).

(C) The normalized capacities versus aging cycles of second-life batteries in dataset 2 under constant temperature and variable temperatures.

(D) The capacities versus aging cycles in dataset 3 with different current rates and temperatures.

(E) The capacities versus aging cycles in dataset 4 with different current rates and temperatures.

(F) The capacities versus aging cycles in dataset 5 under room temperature with 1/3C current in the whole lifespan.

applications where the constant current condition (which is generally experimented in the lab) is used for the estimations under dynamic current conditions with variable temperatures (close to field data), and only three sparsely labeled samples from the first 10% data of the test batteries are used. The results in Figure 3A show that the initial model can be used to estimate the SOH of batteries aging under different dynamic working profiles through a domain adaptative continual learning process. Estimation errors show that most entries fall in the range of [−0.04, 0.01]. When the model is applied for the SOH estimation of batteries operating under dynamic working profiles and/or variable temperatures (the results in Figure 3B), estimations are still stable and converged to the real values although more outliers appear. The estimation errors are mostly within [−0.04, 0.02], and more than half fell in [−0.01, 0.01]. The R square (R^2) between the estimated SOH and the real SOH is larger than 0.87. Both estimations show significant improvement in the accuracy and convergency to the results obtained by the initial base model (the results shown in Figure S2), which indicates that our model can quickly suit different application scenarios through only unlabeled and very few labeled data for continual learning.

The estimations for the batteries in the second lifespan under constant temperature and variable temperatures are shown in Figures 3C and 3D, indicating that our model also meets the accuracy and reliability requirements. The R^2 between the estimations and

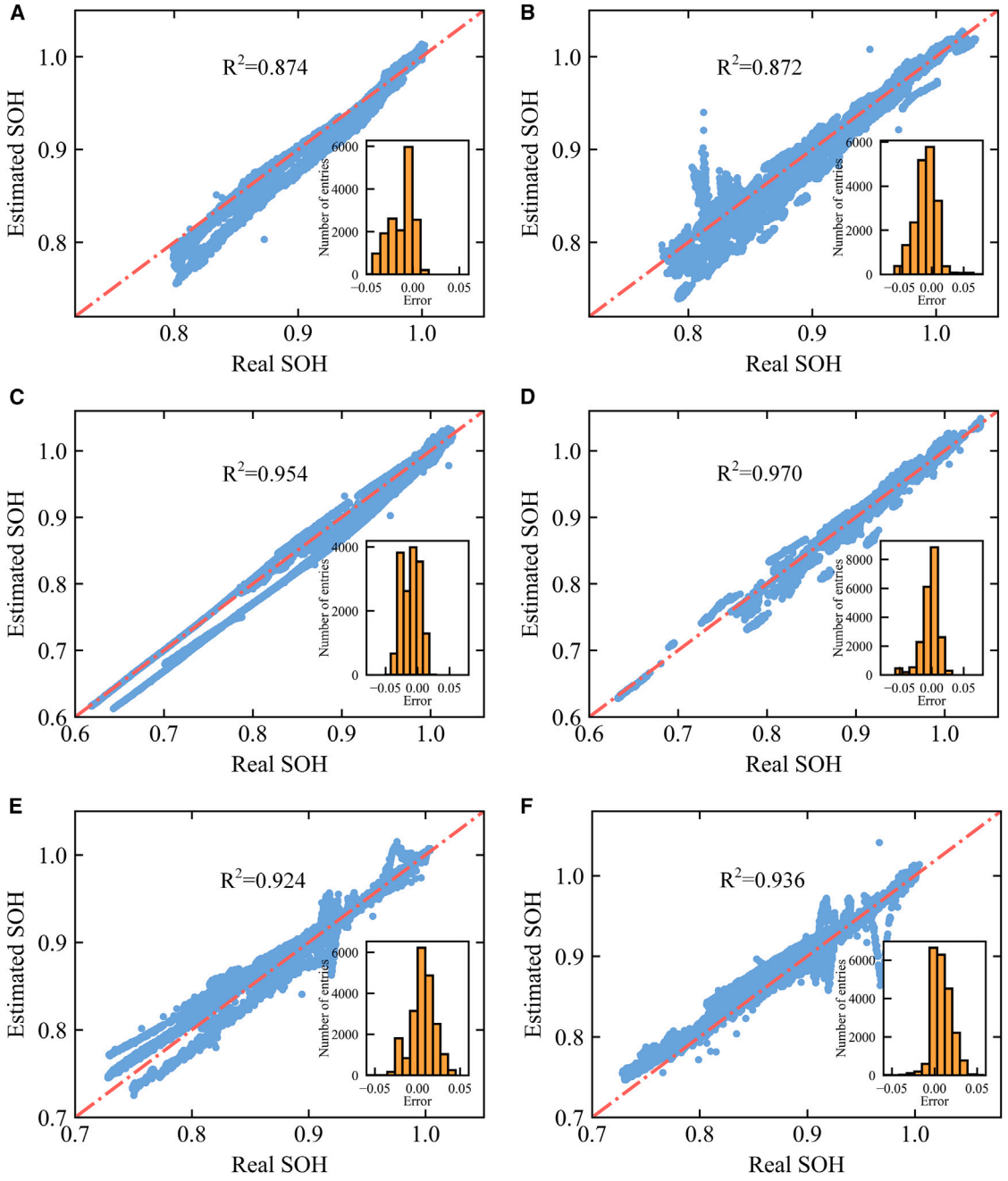

Figure 3. Results of SOH estimations for batteries aged under various conditions

(A) Estimated SOH and estimated errors for batteries in dataset 1 aged under constant temperature with dynamic discharge profiles.

(B) Estimated SOH and estimated errors for batteries in dataset 1 aging under variable temperatures with dynamic discharge profiles.

(C) Estimated SOH and estimated errors for secondary life batteries in dataset 2 aged under constant temperature.

(D) Estimated SOH and estimated errors for secondary life batteries in dataset 2 aging under variable temperatures.

(E) Estimated SOH and estimated errors for batteries in dataset 3 aged under different current rates and temperature conditions using only cell 2 (1C/25°C) for base model training.

(F) Estimated SOH and estimated errors for batteries in dataset 3 aged under different current rates and temperature conditions using only cell 6 (1C/35°C) for base model training. Our model trained by one battery aged under constant temperature and constant current can be used to estimate the SOH under various conditions with most errors less than 0.04 (99.75% for 114,741 entries in total), which shows great improvement to the base model (Figure S2) using a few early data for continual learning.

the real values is larger than 0.95, and the estimated errors are mostly within [−0.03, 0.02]. The estimation results using the initial base model are shown in Figure S2, which have larger errors than our model. In short, the estimations meet the accuracy and reliability requirement satisfactorily under both dynamic discharge current and constant discharge current, both the constant temperature and dynamic temperatures, and in both primary life batteries and secondary life batteries.

The batteries in the third dataset are aged under different constant temperatures using constant currents with different rates. Batteries aged in dataset 3 have a large capacity (100 Ah), which makes them suitable for heavy duty EVs and grid storage stations. We evaluate our model using one battery aged under one specific current rate and temperature to estimate the SOH of other batteries aged with other current rates and temperatures. Batteries using a common aging scenario with 1 C current under 25°C (cell 2 in dataset 3) and 1 C current under 35°C (cell 6 in dataset 3) are used to build the initial base model to estimate other batteries through continual learning using early information, and the results are shown in Figures 3E and 3F, respectively. The estimated values converge to the real values satisfactorily with R^2 of 0.924 and 0.936, respectively. Similarly, most errors are less than 0.04, indicating accurate and robust estimations across a wide temperature range (25°C–55°C) and different current rates. The estimations based on the base model are shown in Figures S2E and S2F, where the results show that only a few estimated values converge to the real values while the majority diverge, indicating the poor generalization of conventional data-driven models.

Feature distribution interpretation

Lack of interpretation in most data-driven methods such as "black boxes" causes difficulties in understanding the mechanisms behind their performance. In contrast, our method tried to interpret the model performance by looking inside the developed data-driven model using the post hoc analysis strategy. The hidden states are critical information for the final output, i.e., the estimations of the neural network model. Therefore, we demonstrate the distribution of the hidden states, referring to the node values, in the same layer for both source and target batteries in our work to explain the model performance. The output distribution of the domain adaptative layer for the batteries in the target domain and source domain are shown in Figures 4A–4C for datasets 1, 2, and 3, respectively. The output distributions of the same layer in the initial base model and the updated model using the fine-tuning strategy with newly obtained labeled data from the target battery[45–47] are shown in Figures 4D–4F and 4G–4I, respectively. The comparison in Figure 4 demonstrates that the distribution of the hidden states has nearly perfect overlaps in our model, which gives an interpretation of why the model performs satisfactorily in both source and target domains. The hidden state's distribution of the base model shows domain discrepancies between the target and source batteries, which makes the model fail to have high accuracy and reliability on the target batteries. As for fine-tuning strategy-based models, the distributions also show discrepancies, which improve the model performance on the target battery but deteriorate the performance on the source battery (further discussed in the following section). As a result, our model can be regarded as a "gray box," where the hidden state distributions help interpret the model performance properly despite the unknown physical meaning of these hidden states.

Continual learning ability

A major limitation to the generalization of data-driven models used is the "catastrophic forgetting." On the contrary, our model can continually learn new aging

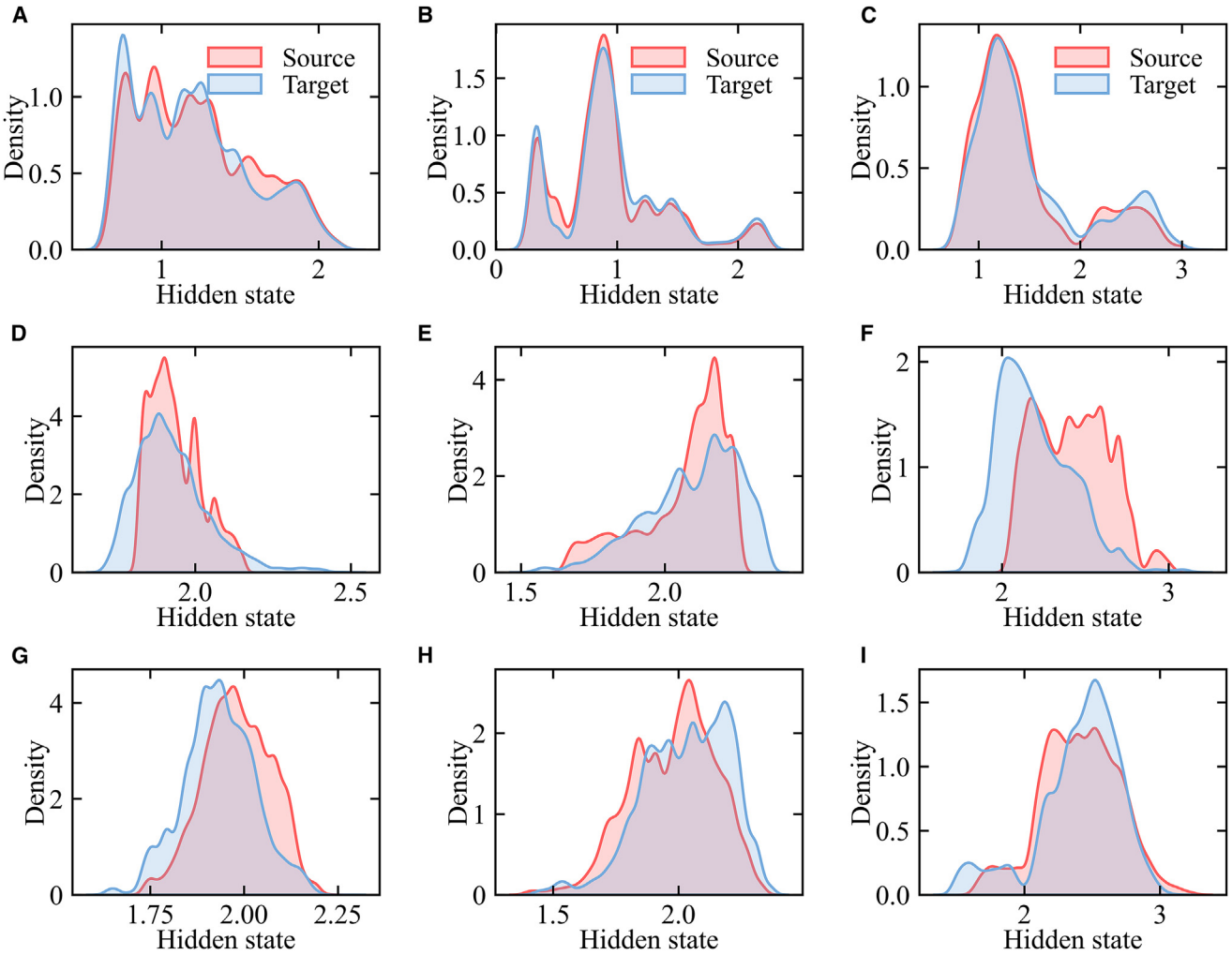

Figure 4. Hidden state distributions interpretation

(A–C) The distribution of the hidden states outputted by the domain adaptative layer for the source batteries and target batteries based on our model in datasets 1, 2, and 3, respectively.

(D–F) The distribution of the hidden states outputted by the same layer for the source batteries and target batteries based on the base model in datasets 1, 2, and 3, respectively.

(G–I) The distribution of the hidden states outputted by the same layer for the source batteries and target batteries based on the purely fine-tuned model in datasets 1, 2, and 3, respectively. The state distribution of the target domain overlaps better in our model, which enables satisfactory estimations of the target batteries while maintaining the performance of the source batteries.

information while maintaining the ability to estimate the health of batteries that have similar aging conditions to the learned information before. We use dataset 3 for the demonstration and evaluation since different temperatures cause obviously different degradation patterns, as shown in Figure 2. The estimation results are shown in Figure 5. First, the initial base model trained by cell 2 (aged with 1C under 25°C) is used to estimate the SOH of all batteries aged with 1C under 35°C and 55°C, and 0.3C under 35°C, the results could be seen from Figure 5A. Then, the sparse data of this battery are stored in the data storage buffer to continually train the model with domain adaptation using sparsely labeled data and unlabeled data collected from early stages from one battery aging under 35°C. Then the updated model is again used for the estimation of all batteries, as shown in Figure 5B. After that, sparse data from one battery aging under 1C/55°C and 0.3C/35°C are

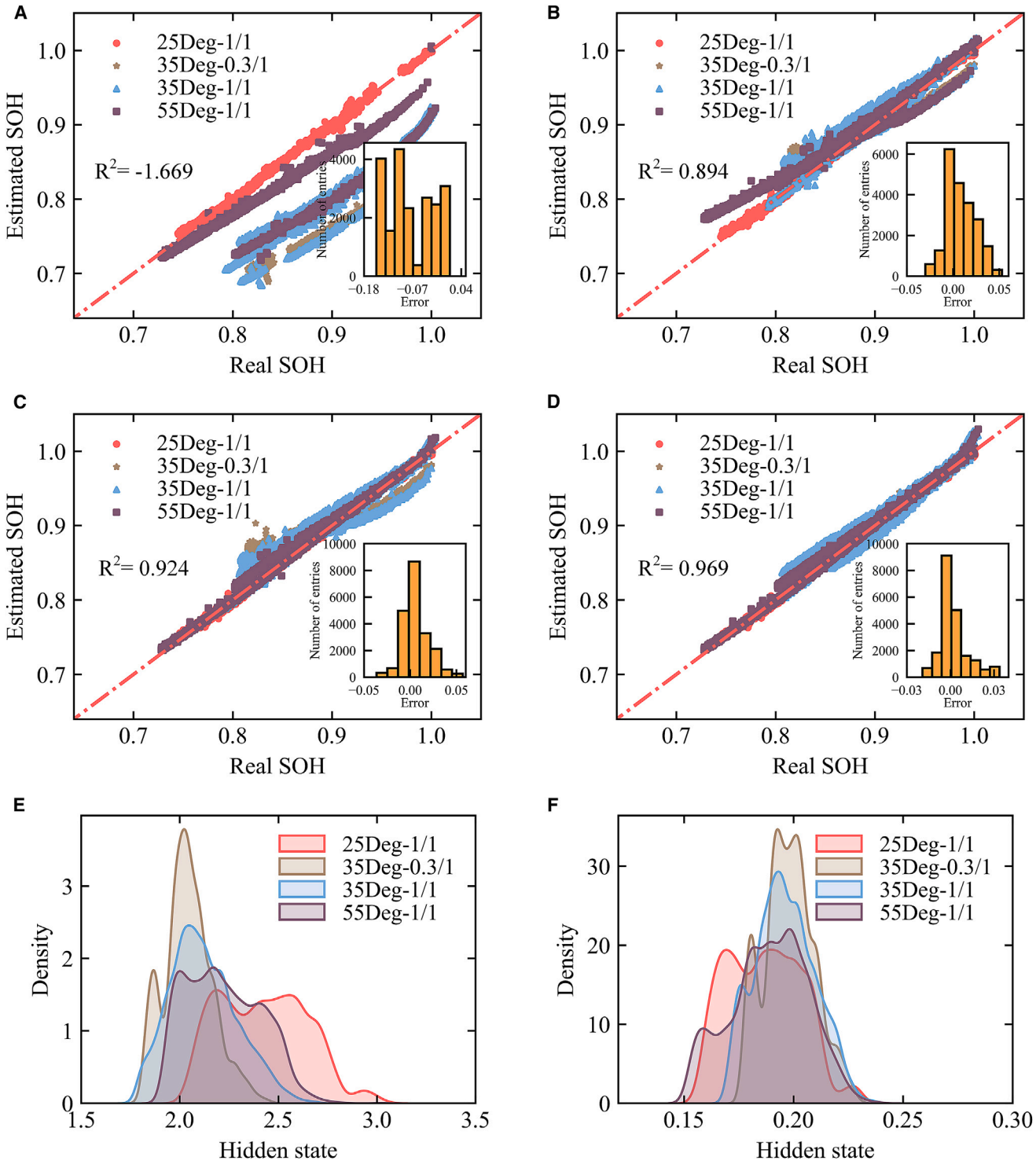

Figure 5. Continual learning evaluations

(A and B) (A) Estimated SOH and estimated error of batteries in dataset 2 with the initial base model trained using data from 1C/25°C. (B) Estimated SOH and estimated errors of batteries in dataset 2 with continual learning using data from a battery aging under 1C/35°C based on the model from (A).

(C) Estimated SOH and estimated errors of batteries in dataset 2 with continual learning using data from a battery aging under 1C/55°C based on the model from (B).

(D) Estimated SOH and estimated errors of batteries in dataset 2 with continual learning using data from a battery aging under 0.3C/35°C based on the model from (C).

Figure 5. *Continued*

(E) Hidden states distribution of batteries aging under different scenarios from the model in (A).

(F) Hidden states distribution of batteries aging under different scenarios from the model in (D). Our model has a good ability to learn the aging information with the availability of limited data from different scenarios while maintaining satisfactory performance on the previously learned scenarios, which enables our model to cover more estimation requirements and ensure the feature distributions converge to similar distributions.

continually used to update our model, whose estimation performances on all batteries are shown in Figures 5C and 5D, respectively. Our model continually learned new aging information under different scenarios while maintaining the previously learned information successfully, so that the accuracy and generalization are incrementally improved. The R^2 increased from −1.669 to 0.969 from the initial base model to the final model. The main error distribution decreases from [−0.152, 0.014] to [−0.019, 0.034]. The root mean-square error (RMSE) and mean absolute error (MAE) also decrease continually from case A to case D in Figures 5A–5D, as listed in Table S3, where the RMSE and MAE for the final model on the estimation of all the batteries are reduced to 0.959% and 0.629%, respectively, from 8.957% to 7.399%. The comparative results shown in Figures 5E and 5F, which show the hidden state distributions of batteries for various scenarios generated by the initial model and the final updated model, can be used to interpret the model. This explains why the initial model failed for health estimation under various application scenarios and why our model's generalization grew. The feature distributions are almost overlapping, which improves the estimation model's generalization and accuracy under a variety of working conditions. To demonstrate the advantage of our method compared with the existing fine-tuning-based method, which purely uses newly obtained labeled data from the target domain to update the model, the performances of the fine-tuning-based method under the same updating scenarios are shown in Figures S3A–S3C. It demonstrates that, although the fine-tuned model performs better in the target battery after updating the model, it forgets the historically learned characteristics and causes a worse performance in previous estimation scenarios. Therefore, when purely applying the fine-tuning strategy, catastrophic forgetting happens, making the model fail to satisfy the estimations under different scenarios. The hidden states distribution shown in Figure S3D also interprets the reason for this phenomenon after fine-tuning. That is the domain discrepancies between different scenarios still exist, causing poor model performance on the previous tasks. The results are of great value to industrial applications, where the initial model can be built with some experiments in the lab before implementations and be incrementally improved during applications in various unseen working scenarios such as loading profiles and environment temperatures.

Different battery manufacturers

The other two datasets (datasets 4 and 5) are used to evaluate the generalization of our method. The estimation results are shown in Figures S4 and S5. Our model meets the requirement for the estimations under different scenarios with R^2 greater than 0.978 and errors within 0.03 with dataset 4. Dataset 5 contains aging data in a standard current mode under room temperature for the whole lifespan (SOH reduces to less than 0.4). The estimation results shown in Figure S5 indicate accurate and reliable estimations with R^2 larger than 0.996 and errors within 0.05. Therefore, combined with the estimation on all five datasets, our model has satisfactory generalization ability on the application under different battery chemistry and formats, different working profiles, and environmental temperatures.

Comparisons with other transfer learnings

The avoidance of catastrophic forgetting while learning new aging information is one major advantage of our model. We compare our method with other transfer

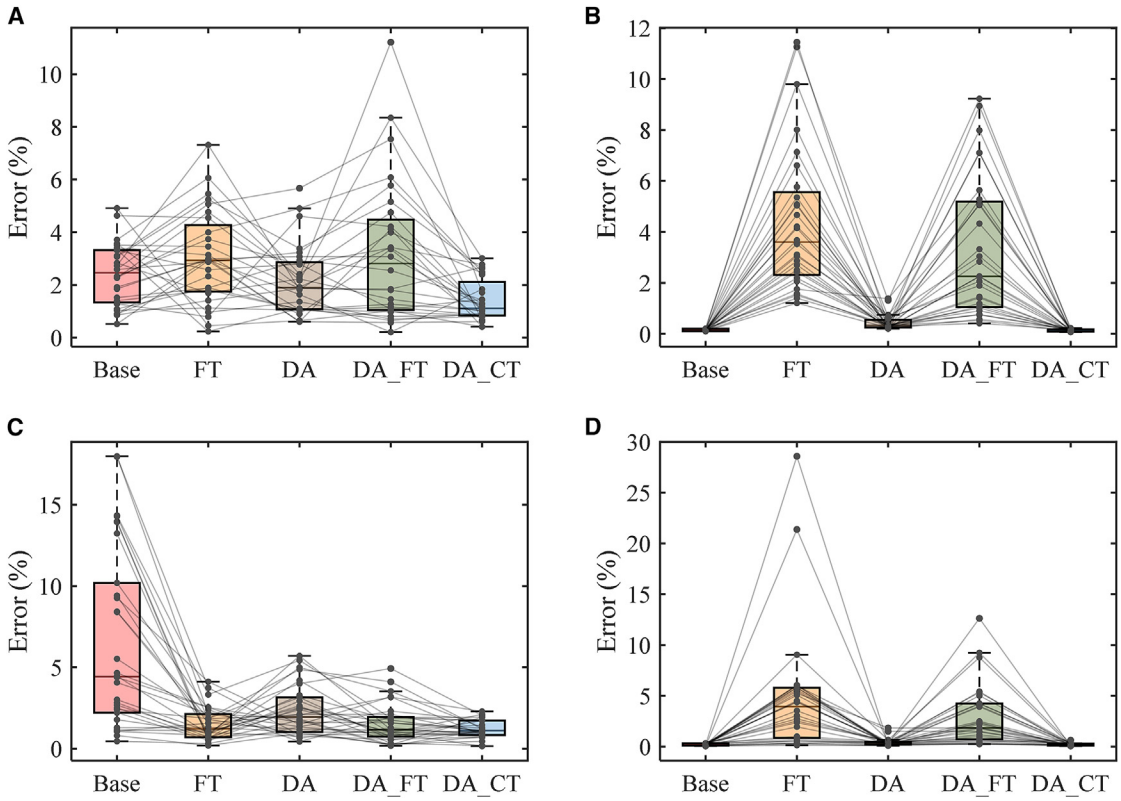

Figure 6. Comparative results with other transfer learnings

(A and B) The estimated RMSE for the target batteries and source batteries for datasets 1 and 2.

(C and D) The estimated RMSE for the target batteries and source batteries for datasets 3 and 4. Compared with the base model and models with other transfer learning strategies, our model shows better accuracy and reliability.

learning strategies to evaluate the accuracy in all estimation scenarios. Fine-tuning and basic domain adaptation are included, where four models in total are included for the comparisons. The meaning of each model is described in Note S3. The RMSE of the target and source batteries in datasets 1 and 2 (results contain the two datasets) are shown in Figures 6A and 6B while the corresponding MAE are shown in Figures S6A and S6B, respectively. It shows that our model has the best performance for the batteries working under different dynamic discharging profiles and variable temperatures with a narrow error distribution, indicating the best accuracy and reliability compared with other models. The RMSE and MAE results for batteries contained in datasets 3 and 4 (results containing the two datasets) are shown in Figures 6C, 6D, S6C, and S6D respectively. In this case, the target batteries have different current rates and different temperatures to the source battery, which causes the base model to have poor accuracy on the target domain. When the information from the batteries is obtained for transfer learning or continual learning, errors are reduced significantly. This indicates from the results that unlabeled data used for reducing domain discrepancies between the source battery and target battery are also beneficial for accuracy improvement. This is because the mapping relationships between the input measurements and output SOH are more adaptable for the testing battery by minimizing the domain discrepancies. Compared with the pure unlabeled data-enabled domain adaptation, sparse limited data help improve the accuracy of the target domain, while pure fine-tuning suffers from catastrophic forgetting. Our model, on the contrary, maintains good performance on

Table 1. Comparative evaluation of our model and other transfer learnings (%)

	RMSE for target domain			MAE for target domain			RMSE for source domain			MAE for source domain		
Case	Mean	Max.	SD	Mean	Max.	SD	Mean	Max.	SD	Mean	Max.	SD
BASE	4.573	17.987	4.562	4.193	17.965	4.475	0.172	0.324	0.087	0.126	0.242	0.067
FT	2.361	11.213	2.218	1.838	8.129	1.700	3.108	12.633	2.869	2.826	12.076	2.679
DA	2.259	5.704	1.412	1.949	5.484	1.274	0.420	1.838	0.339	0.328	1.797	0.321
DA_FT	2.361	11.213	2.218	1.838	8.129	1.700	3.108	12.633	2.869	2.826	12.076	2.679
DA_CT	1.312	3.015	0.682	1.085	2.662	0.628	0.159	0.623	0.102	0.128	0.666	0.107
GPR	3.952	17.959	3.999	3.497	17.938	3.719	0.077	0.199	0.056	0.056	0.147	0.042
RFR	3.930	17.834	3.462	3.549	17.722	3.372	0.039	0.074	0.021	0.026	0.046	0.013
LR	14.758	185.806	35.519	10.784	147.825	27.389	0.129	0.297	0.089	0.095	0.221	0.067
SVR	4.137	23.651	5.170	3.893	23.633	5.121	0.225	0.604	0.181	0.179	0.523	0.163
CNN	6.2151	25.3715	6.4348	5.7801	25.2623	6.3335	0.1894	0.4955	0.1488	0.1390	0.3739	0.1143
LSTM	4.4001	26.9428	5.4930	3.8836	20.7222	4.9787	0.4001	0.5633	0.1475	0.2930	0.4101	0.1125
CNN-LSTM	3.4643	16.3019	3.3709	3.1271	16.2852	3.1825	0.2458	0.4566	0.1345	0.1828	0.3384	0.0996

both the target domain and source domain with the errors located in the smallest range, indicating satisfactory accuracy and reliability. Refer to Figures S7–S11 and Tables S4–S8 for the estimation results of each testing battery cell and the comparisons between different models.

The numerical statistical results for all the batteries are listed in Table 1. Our model has minimal mean and maximum errors, and minimal standard deviation (SD) of error distributions, indicating accurate and reliable estimations on all domains with different aging profiles and temperature conditions. The mean and maximum RMSE for the target domain are 1.312% and 3.015%, respectively, reducing more than three times from the initial base model, while the SD reduced significantly from 4.562 to only 0.682. The improvement of our model compared with other transfer learning strategies is also reflected in Table 1. In addition, four widely used machine learning methods for battery SOH estimation are also included for evaluation, which are LR, SVR, GPR, and random forest regression. As shown in Table 1, like the basic neural network-based method, these four machine learning methods all have good performances on the trained source domain but fail to provide satisfactory estimations for target domains with various application conditions. It is also foreseeable that these models will also suffer from catastrophic forgetting when they are simply updated with newly acquired data such as the fine-tuning strategy. The results with other advanced deep learning models including LSTM, CNN, and CNN-LSTM for the base model construction are also listed in Table 1. The results indicate that CNN-LSTM has better accuracy compared with feedforward NN, LSTM, and CNN for the SOH estimations. While the base model also has poor generalization ability under different working scenarios, reflected by the large maximum values of the RMSE and MAE, from the battery that has diverse degradation patterns. Therefore, the model is still required to be updated during applications, especially under different working conditions to improve the model's accuracy and generalization, which can be achieved by the proposed framework. Therefore, the proposed framework shows priority regarding the performance on both source and target domains compared with conventional machine learning and transfer learning methods. The main objective is to update the model incrementally so that the feedforward NN is applied for the demonstrations. In real applications, the base network can be constructed with different networks. For example, the CNN-LSTM can be used for the base network part under condition data showing poor quality than experimental data, while the proposed framework is generally applicable for the model continually updating during applications.

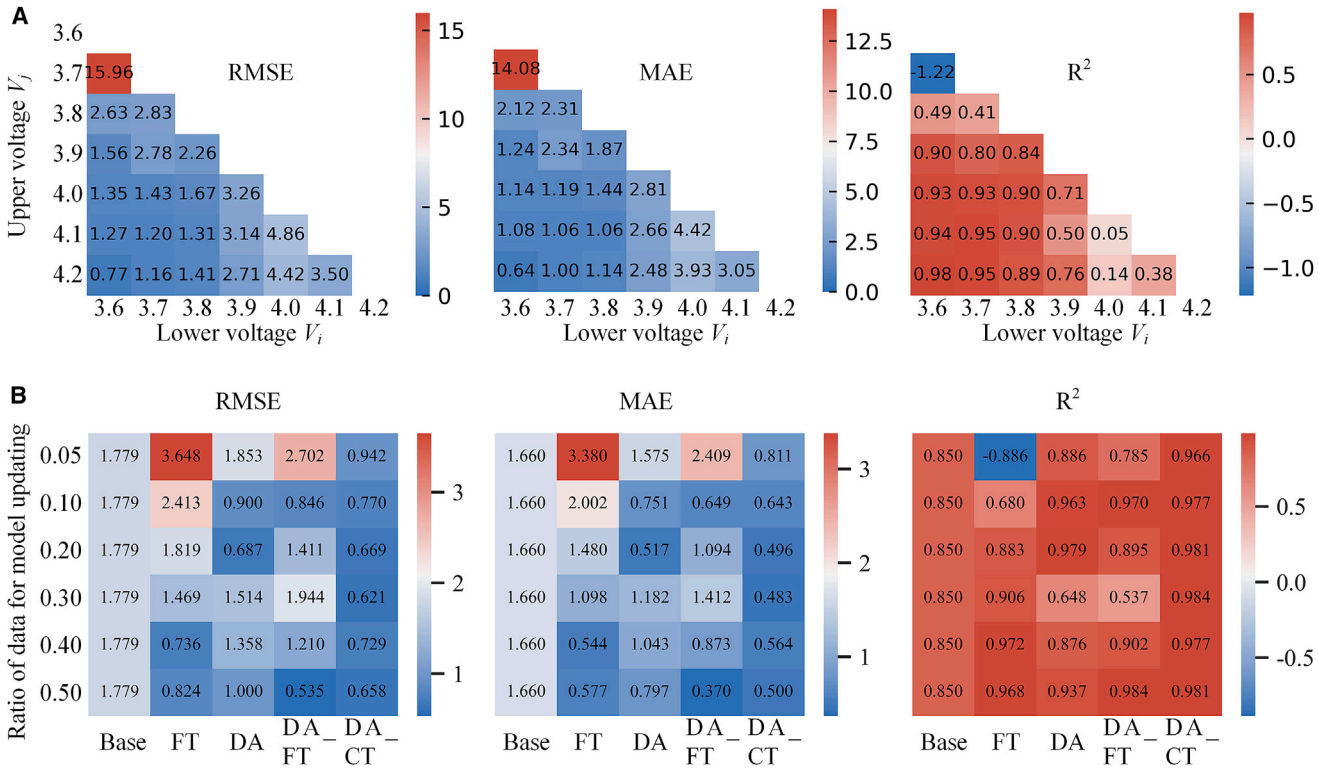

Figure 7. Generalization with a different voltage range for model input and different ratios for continual learning

(A) The estimated mean RMSE, MAE, and fitted R^2 of the three batteries with three kinds of dynamic working profiles with different voltage ranges (V_i and V_j represent the lower voltage and upper voltage in the partial voltage sequence). The results indicate that our model can meet the estimation requirement using data from a voltage range less than 0.1 V in 3 min charging with an error less than 2.78% and fitted R^2 larger than 0.8.

(B) The estimated mean RMSE, MAE, and fitted R^2 for the three batteries in dataset 1 aging under three kinds of dynamic profiles with different ratios of data for model updating. Our model has errors less than 0.94% and fitted R^2 larger than 0.96 with only 5% data for continual learning and maintaining high accuracy with different ratios.

Different voltage ranges and data ratios for model updating

Practical applications usually have a partial charging process and the usually used voltage ranges vary with the real requirement such as in EVs and smart grids. Therefore, it is also significant to evaluate our model under different partial charging conditions for the generalization assessment. We select three batteries aged under three different dynamic profiles to evaluate our model by changing the voltage range from 3.6 to 4.2 V in the first stage charging process. The mean results of the three testing batteries are shown in Figure 7A. It shows that, when the lower voltage is below 3.8 V and the upper voltage is larger than 3.9 V, our model realizes RMSE and MAE less than 2.78% and the fitting R^2 is larger than 0.8. When the upper voltage is larger than 4.0 V, the errors are reduced to less than 1.67% while the R^2 is larger than 0.9. Considering the charging process of the battery in dataset 1, as shown in Figure S12, the charging time between 3.8 and 3.9 V in the first charging stage is less than 3 min and the charging time between 3.8 and 4.0 V is less than 4 min, which enables our model to be used in practical applications using short-term charging data.

We evaluate our model and other transfer learning models with the increase of ratio for model updating, and the mean values are shown in Figure 7B. The results on the source batteries are shown in Figure S13. The results indicate that our model quickly reduces the errors to less than 0.942% and increase the R^2 to larger than 0.966 even

with only 5% ratio of data for model updating, where only two sparsely labeled samples are used. Compared with other transfer learning strategies that may have poor performance under some scenarios, our model maintains high performance in all cases. Therefore, from the evaluations of different voltage ranges and available data rations, the model has promising industrial application abilities under random depths of discharges during their whole lives. The batter health estimation model can still be incrementally improved based on the proposed framework.

Full life estimation

Finally, we evaluate our model on the estimation for the full lifespan. In the above sections, the estimation results of dataset 5 indicate that our model provides accurate estimations for the whole lifespan. Here, we use the battery in dataset 1 to estimate the second-life battery application in dataset 2, which is the same battery but with a different aging profile retired from dataset 1. The results shown in Figure S14 indicate that our model has better accuracy than other models, meeting the estimation requirement for the second-life battery by taking advantage of information gathered from the primary-life battery. This is significant for practical applications since it is assumed that many batteries are retired from EVs to be implemented in smart grids, etc., and the model developed in our method shows great application potential to continually learn the aging information to meet the health estimation for health estimation of second-life batteries.

DISCUSSION

We developed a data-driven model for battery health estimation based on domain adaptative continual learning to solve the natural challenges of low generalization, the large requirement of labeled data, catastrophic forgetting, and poor interpretation. Our model is initially built using the data collected from one common aging test and can be adopted for the estimation under unknown conditions with only unlabeled data and sparsely limited labeled data at early stages, where the RMSE is less than 0.95 and the R^2 is larger than 0.96 under the case with only two sparsely labeled samples from the first 5% aging data, indicating data efficient for the modeling. With three sparsely labeled samples collected from the first 10% aging data, our model achieves the most absolute errors of less than 5% despite different battery chemistry and formats, different aging profiles and current rates, and different environmental temperatures, with only one battery used for initial modeling. The proposed method is valuable for industrial applications, where the initial model can be constructed via some lab data and be continually improved with unlabeled data and sparsely labeled data obtained during usage to incrementally improve the model generalization.

Our model is interpreted by post hoc analysis, and succeeds in reducing the domain discrepancy between the source domain and target domain that interprets the satisfactory estimation performances. Our model is continuously improved with the availability of both unlabeled and labeled data from unknown conditions while maintaining the performance on previous tasks, which avoids catastrophic forgetting. Compared with other transfer learning strategies, both the unlabeled data and labeled data from the target batteries are well used for model improvement. Our model has better accuracy and generalization under different testing scenarios, with a mean RMSE of only 1.312%, and even the worst testing achieves an RMSE of only 3.015%. Our model is also more reliable to the different ratios of data used for learning compared with other transfer learnings. Finally, our model also supports estimations using shallow partially charged data within 3 min for a mean

RMSE of less than 2.78% under three typical dynamic discharging scenarios and achieves a mean RMSE of 1.67% with data collected within 4 min. Our model is a general framework that can be easily extended to modeling with other neural networks and with a feature-based method. Therefore, our model is promising for implementation in onboard applications.

The proposed method shows satisfactory performance on the health estimations under different application scenarios. However, there are still some limitations that need to be addressed in future work. Firstly, there are some local large errors existing in the estimations due to the quality of measured data and the quick change of environmental situations. In future work, the physics information from the electrochemical model is supposed to be integrated to reduce these errors and further improve the generalization and interpretability by explaining with physical aging mechanism. Secondly, the preset manually tailed transfer weight is used in this paper for domain adaptation, and the overall performance considering all the testing scenarios has been significantly improved. One specific value for all testing scenarios also tells the strategy is general and avoids biased results with carefully selected weight for each specific testing scenario. However, it cannot be optimal for all the specific conditions, indicating a more intelligent optimization method is worth investigating to adapt the best choice of transfer weight under different scenarios during training the model with optimization methods. Finally, the extrapolation to other types of batteries such as all solid batteries, and Li-sulfur batteries, and the implementation in battery packs are valuable to evaluate the effectiveness of the proposed framework.

EXPERIMENTAL PROCEDURES

Resource availability

Lead contact

Further information and requests for resources and materials should be directed to and will be fulfilled by the lead contact, Xiaosong Hu (xiaosonghu@ieee.org).

Materials availability

This study did not generate any unique materials.

Data and code availability

The data generated in this study can be found at https://data.mendeley.com/datasets/n3b54nsw8m/2. Additional raw data may be available upon reasonable request.

Battery cycling and data preparation

Experiments for the aging of several commercial batteries are conducted in this paper for the verification of the proposed method. The first is ultra-fast charging followed by a dynamic discharging profiles-based battery dataset. To the best knowledge of the authors, this is the first public dataset with different dynamic discharging profiles to age the batteries until end of life. Different dynamic profiles are included, which are urban dynamic profile, highway profile, and hybrid profile. The current load of each profile and the corresponding voltage are shown in Figure S15. Two cycles of the dynamic current lasting 24 min are used. The mean current is set to ensure that the three dynamic loadings have similar throughput during this period. Two different time periods are considered to load the dynamic currents, which makes the dynamic loading conducted at two different state of charge (SOC) stages. One battery aging under the constant current is used as the benchmark to illustrate the types of current on the aging influence of batteries. To make the experiment

closer to the practical applications, another batch is conducted on the periodically changed temperatures varied from 25°C–35°C to 25°C–15°C, which emulates the influence of seasonal variations on battery aging.[60] Again, this is the first dataset conducted on the changeable environmental temperatures to the best knowledge of the authors, where the degradation trajectories are varied with environmental temperatures during aging. The normalization is conducted by calculating the ratio of the current available capacity to the fresh capacity (starting from 25°C), which makes the demanded estimation of current capacity to be easily obtained by multiplying the estimated SOH with the fresh capacity. There are 15 batteries in total in this dataset, whose capacity curves are shown in Figure 2. The second dataset is the same batteries from the first dataset, which are used for the constant current discharging after the batteries retired from dataset 1. These batteries are now considered second-life batteries. The CC-CV charging and CC discharging are conducted to continually age the batteries. Similarly, constant environment temperature and changeable temperatures are considered. The first two datasets are collected from the pouch batteries. The third and fourth dataset is collected from the aging experiment conducted on the prismatic cells with 100 Ah. Most of the public datasets are aging on cylindrical batteries, while prismatic batteries are also popular in real applications for both electric transportation and energy storage stations. We aged these batteries with different current rates and environmental temperatures to generate data seen in different application scenarios. The last battery dataset is collected by aging the small polymer batteries from fresh to SOH less than 0.4 for the study of SOH estimation over the entire lifetime.

The feature-free method is adopted in our model, where the partially charged *Q*-*V* curve is selected as input information. Note that the incomplete charging/discharging process when starting the test from reset is deleted. The abnormal data such as a larger difference between the sample from previous and later data are filtered with a moving average. The raw measured data changed with battery aging, which caused the *Q*-*V* curve to be unaligned. Therefore, the interpolation method is used to obtain the *Q*-*V* curve in a certain voltage range, where linear interpolation is adopted. To ensure the online application, the partial voltage range is used, where [3.6, 4.2] is selected as the initial voltage range for NCA and polymer batteries while [3.3, 3.5] is used for LFP batteries with a voltage interval of 5 and 2 mV for interpolation to ensure the same input length. The voltage ranges can also be reduced considering the specific applications and are evaluated in the results.

Machine learning model

For the end-to-end health estimation, the measured data of partial charging *Q*-*V* sequences are needed for the input while the SOH is the output. For the purpose of using a simple model to demonstrate the proposed model while also guaranteeing the estimation performance, a feedforward neural network with backward propagation is adopted, where two hidden layers and an output layer are included. The design of the framework is described in Figure S16. The source labeled data from one battery, stored sparse data in previous tasks, and sparsely labeled data from the target battery are used to train the model by minimizing the mean square error loss of the output layer and the maximum mean discrepancy (MMD) loss of the domain adaptive layer simultaneously. To interpret the model performance based on the post hoc analysis, the distribution of hidden states of the domain adaptative layer is also illustrated. Domain discrepancies would cause divergent distributions of hidden states in the source domain and target domain, leading to the poor generalization ability of conventional machine learning models. By analyzing the distributions of hidden states in both the source and target domain, we find the interpretations for the

high performance of our model under different scenarios. It should be noted that the bottleneck layer can be changed to other machine learning models such as CNN, LSTM, CNN-LSTM, etc., which are widely used networks in battery health prognostics, and the implementations of these machine learning models are also provided for reference. The hyperparameters and settings of the neural network are listed in Note S4. The basic calculation of a neuron in fully connected layers by the weight w, bias b, and states h from the former layer is denoted as,

$$y = \sum_{i=1}^{N} w_i h_i + b_i \quad \text{(Equation 1)}$$

The first hidden layer is set as a sharing layer while the second hidden layer is set as a domain adaptative layer, where the MMD is calculated between the hidden states of the source battery and target battery as a loss that needs to be reduced. The MMD is a measure of the difference between two probability distributions in the mean embedding of the features.[61] Given two samples in two datasets $X = \{x_i\}_{i=1}^{n_1}$ and $Y = \{y_i\}_{i=1}^{n_2}$, the MMD between the X and Y could be expressed as,[62]

$$MMD_H(X,Y) = \sup_{\Phi \in H}\left(E_P[\Phi(x)] - E_q[\Phi(y)]\right) \quad \text{(Equation 2)}$$

where H represents a reproducing kernel Hilbert space (RKHS), $\Phi(\cdot)$ is a nonlinear mapping function from raw data space to the RKHS space, and p and q are the probability distributions of generating the two datasets. The empirical approximation to the MMD can be denoted as follows,[42,63]

$$MMD_H^2(X,Y) = \left\| \frac{1}{n_1}\sum_{i=1}^{n_1}\Phi(x_i) - \frac{1}{n_2}\sum_{j=1}^{n_2}\Phi\left(y_j\right) \right\|_H^2 \quad \text{(Equation 3)}$$

The kernel trick is then used to get the expression,[42]

$$MMD_H^2(X,Y) = \frac{1}{n_1^2}\sum_{i=1}^{n_1}\sum_{j=1}^{n_2}k(x_i,x_j) - \frac{2}{n_1 n_2}\sum_{i=1}^{n_1}\sum_{j=1}^{n_2}k\left(x_i,y_j\right) + \frac{1}{n_2^2}\sum_{i=1}^{n_1}\sum_{j=1}^{n_2}k\left(y_i,y_j\right) \quad \text{(Equation 4)}$$

where $k(\cdot,\cdot)$ is the kernel function of the RKHS. In this paper, the Gaussian radial basis function is used,[42]

$$k\left(x_i,y_j\right) = e^{\frac{\left(-\left\|x_i - y_j\right\|^2\right)}{2\gamma^2}} \quad \text{(Equation 5)}$$

The final loss function during continual learning is constructed as follows

$$L = \sum L_{MSE} + \lambda L_{MMD} \quad \text{(Equation 6)}$$

During the initial base training and fine-tuning using labeled data, the MMD loss is set as 0 and only the MSE loss is considered to train the neural network. In the domain adaptation process, the MSE loss of the source battery, and the MMD loss of the domain discrepancy between the source battery and target battery of the domain adaptative layer are reduced during training. The weight factor of MMD loss is set as 0.01 for all the testing cases for the generalization of our model. The Adam optimization method is used to train the model and the early stopping strategy is adopted to avoid overfitting. The RMSE, MAE, and R^2 are used for the accuracy evaluations of the estimation results, which are defined as follows.

$$RMSE = \sqrt{\frac{1}{N}\sum_{i=1}^{N}(y_i - z_i)^2}, \quad \text{(Equation 7)}$$

$$MAE = \frac{1}{N}\sum_{i=1}^{N}|y_i - z_i|, \quad \text{(Equation 8)}$$

$$R^2 = 1 - \frac{\sum_i (y_i - z_i)^2}{\sum_i (y_i - \overline{y}_i)^2}, \quad \text{(Equation 9)}$$

where y represents the true value and z is the estimated value while $\overline{y}$ is the mean value of all the true values. During model training, one source battery is firstly used for the initial model training, then the unlabeled data and limited labeled data from the target batteries are used for the domain adaptative continual learning to update the model to improve the generalization under different scenarios. Therefore, the model is incrementally updated from the beginning to the various applications. Note that the cross-validation is used during the initial model training and is not applied during subsequent model updating, since only very limited labeled data is available in the testing scenarios. Besides, early stooping is also adopted to help avoid overfitting. The specific cell that serves as the source battery is listed in Tables S4–S8 in each test.

SUPPLEMENTAL INFORMATION

Supplemental information can be found online at https://doi.org/10.1016/j.xcrp.2023.101743.

ACKNOWLEDGMENTS

The work of X.H. was funded by the National Key Research and Development Program (grant no. 2022YFB3305403), the project of basic research funds for central universities (grant no. 2022CDJDX-006), the Natural Science Foundation of China (grant nos. 52111530194 and 72361137006), , and the Talent Plan Project of Chongqing (grant no. cstc2021ycjh-bgzxm0295). The work of R.T. was funded by the "SMART BATTERY" project, granted by Villum Foundation in 2021 (project no. 222860).

AUTHOR CONTRIBUTIONS

Y.C. conceived the study, carried out the experiments, analyzed the data, developed the model, and wrote the paper. Y.C. and Y.Z. prepared the first and revised drafts. Y.C., Y.Z., S.O., X.H., and R.T. discussed the results and commented on the manuscript. R.T., and X.H. supervised the work.

DECLARATION OF INTERESTS

The authors declare no competing interests.

Received: September 7, 2023
Revised: October 24, 2023
Accepted: November 20, 2023
Published: December 12, 2023

REFERENCES

1. Jiang, B., Gent, W.E., Mohr, F., Das, S., Berliner, M.D., Forsuelo, M., Zhao, H., Attia, P.M., Grover, A., Herring, P.K., et al. (2021). Bayesian learning for rapid prediction of lithium-ion battery-cycling protocols. Joule *5*, 3187–3203.

2. Attia, P.M., Grover, A., Jin, N., Severson, K.A., Markov, T.M., Liao, Y.H., Chen, M.H., Cheong, B., Perkins, N., Yang, Z., et al. (2020). Closed-loop optimization of fast-charging protocols for batteries with machine learning. Nature *578*, 397–402.

3. Chen, B.R., Kunz, M.R., Tanim, T.R., and Dufek, E.J. (2021). A machine learning framework for early detection of lithium plating combining multiple physics-based electrochemical signatures. Cell Rep. Phys. Sci. *2*, 100352.

4. Palacín, M.R., and De Guibert, A. (2016). Batteries: Why do batteries fail? Science *351*.

5. Weng, A., Mohtat, P., Attia, P.M., Sulzer, V., Lee, S., Less, G., and Stefanopoulou, A. (2021). Predicting the impact of formation protocols

on battery lifetime immediately after manufacturing. Joule *5*, 2971–2992.

6. Zhu, J., Xu, W., Knapp, M., Dewi Darma, M.S., Mereacre, L., Su, P., Hua, W., Liu-Théato, X., Dai, H., Wei, X., et al. (2023). A method to prolong lithium-ion battery life during the full life cycle. Cell Rep. Phys. Sci. 101464.

7. Che, Y., Hu, X., Lin, X., Guo, J., and Teodorescu, R. (2023). Health prognostics for lithium-ion batteries: mechanisms, methods, and prospects. Energy Environ. Sci. *16*, 338–371.

8. Börner, M.F., Frieges, M.H., Späth, B., Spütz, K., Heimes, H.H., Sauer, D.U., and Li, W. (2022). Challenges of second-life concepts for retired electric vehicle batteries. Cell Rep. Phys. Sci. *3*, 1–19.

9. Ng, M.F., Zhao, J., Yan, Q., Conduit, G.J., and Seh, Z.W. (2020). Predicting the state of charge and health of batteries using data-driven machine learning. Nat. Mach. Intell. *2*, 161–170.

10. Harper, G., Sommerville, R., Kendrick, E., Driscoll, L., Slater, P., Stolkin, R., Walton, A., Christensen, P., Heidrich, O., Lambert, S., et al. (2019). Recycling lithium-ion batteries from electric vehicles. Nature *575*, 75–86.

11. Kim, S., Yi, Z., Kunz, M.R., Dufek, E.J., Tanim, T.R., Chen, B.R., and Gering, K.L. (2022). Accelerated battery life predictions through synergistic combination of physics-based models and machine learning. Cell Rep. Phys. Sci. *3*, 101023.

12. Reniers, J.M., Mulder, G., and Howey, D.A. (2019). Review and Performance Comparison of Mechanical-Chemical Degradation Models for Lithium-Ion Batteries. J. Electrochem. Soc. *166*, A3189–A3200.

13. Li, J., Landers, R.G., and Park, J. (2020). A comprehensive single-particle-degradation model for battery state-of-health prediction. J. Power Sources *456*, 227950.

14. Hu, X., Xu, L., Lin, X., and Pecht, M. (2020). Battery Lifetime Prognostics. Joule *4*, 310–346.

15. Ali, M.U., Kallu, K.D., Masood, H., Niazi, K.A.K., Alvi, M.J., Ghafoor, U., and Zafar, A. (2021). Kernel recursive least square tracker and long-short term memory ensemble based battery health prognostic model. iScience *24*, 103286.

16. Sun, Y., Ayalasomayajula, S.M., Deva, A., Lin, G., and García, R.E. (2022). Artificial intelligence inferred microstructural properties from voltage–capacity curves. Sci. Rep. *12*. 13421–11.

17. Roman, D., Saxena, S., Robu, V., Pecht, M., and Flynn, D. (2021). Machine learning pipeline for battery state-of-health estimation. Nat. Mach. Intell. *3*, 447–456.

18. Zhang, Y., Tang, Q., Zhang, Y., Wang, J., Stimming, U., and Lee, A.A. (2020). Identifying degradation patterns of lithium ion batteries from impedance spectroscopy using machine learning. Nat. Commun. *11*. 1706–11.

19. Gasper, P., Schiek, A., Smith, K., Shimonishi, Y., and Yoshida, S. (2022). Predicting battery capacity from impedance at varying temperature and state of charge using machine learning. Cell Rep. Phys. Sci. *3*, 101184.

20. Jones, P.K., Stimming, U., and Lee, A.A. (2022). Impedance-based forecasting of battery performance amid uneven usage. Nat. Commun. *13*, 4806.

21. Zhu, J., Wang, Y., Huang, Y., Bhushan Gopaluni, R., Cao, Y., Heere, M., Mühlbauer, M.J., Mereacre, L., Dai, H., Liu, X., et al. (2022). Data-driven capacity estimation of commercial lithium-ion batteries from voltage relaxation. Nat. Commun. *13*. 2261–10.

22. Meng, J., Cai, L., Stroe, D.I., Huang, X., Peng, J., Liu, T., and Teodorescu, R. (2022). An Automatic Weak Learner Formulation for Lithium-Ion Battery State of Health Estimation. IEEE Trans. Ind. Electron. *69*, 2659–2668.

23. Che, Y., Deng, Z., Li, P., Tang, X., Khosravinia, K., Lin, X., and Hu, X. (2022). State of health prognostics for series battery packs: A universal deep learning method. Energy *238*, 121857.

24. Che, Y., Zheng, Y., Wu, Y., Sui, X., Bharadwaj, P., Stroe, D.I., Yang, Y., Hu, X., and Teodorescu, R. (2022). Data efficient health prognostic for batteries based on sequential information-driven probabilistic neural network. Appl. Energy *323*, 119663.

25. Deng, Z., Hu, X., Xie, Y., Xu, L., Li, P., Lin, X., and Bian, X. (2022). Battery health evaluation using a short random segment of constant current charging. iScience *25*, 104260.

26. Ruan, H., Chen, J., Ai, W., and Wu, B. (2022). Generalised diagnostic framework for rapid battery degradation quantification with deep learning. Energy and AI *9*, 100158.

27. Tagade, P., Hariharan, K.S., Ramachandran, S., Khandelwal, A., Naha, A., Kolake, S.M., and Han, S.H. (2020). Deep Gaussian process regression for lithium-ion battery health prognosis and degradation mode diagnosis. J. Power Sources *445*, 227281.

28. Wang, Z., Yuan, C., and Li, X. (2021). Lithium Battery State-of-Health Estimation via Differential Thermal Voltammetry with Gaussian Process Regression. IEEE Transactions on Transportation Electrification *7*, 16–25.

29. Feng, X., Weng, C., He, X., Han, X., Lu, L., Ren, D., and Ouyang, M. (2019). Online State-of-Health Estimation for Li-Ion Battery Using Partial Charging Segment Based on Support Vector Machine. IEEE Trans. Veh. Technol. *68*, 8583–8592.

30. Li, X., Wang, Z., and Yan, J. (2019). Prognostic health condition for lithium battery using the partial incremental capacity and Gaussian process regression. J. Power Sources *421*, 56–67.

31. Duan, Y., Tian, J., Lu, J., Wang, C., Shen, W., and Xiong, R. (2021). Deep neural network battery impedance spectra prediction by only using constant-current curve. Energy Storage Mater. *41*, 24–31.

32. Tian, J., Xiong, R., Chen, C., Wang, C., Shen, W., and Sun, F. (2023). Simultaneous prediction of impedance spectra and state for lithium-ion batteries from short-term pulses. Electrochim. Acta *449*, 142218.

33. Severson, K.A., Attia, P.M., Jin, N., Perkins, N., Jiang, B., Yang, Z., Chen, M.H., Aykol, M., Herring, P.K., Fraggedakis, D., et al. (2019). Data-driven prediction of battery cycle life before capacity degradation. Nat. Energy *4*, 383–391.

34. Vilsen, S.B., and Stroe, D.I. (2021). Battery state-of-health modelling by multiple linear regression. J. Clean. Prod. *290*, 125700.

35. Che, Y., Deng, Z., Tang, X., Lin, X., Nie, X., and Hu, X. (2022). Lifetime and aging degradation prognostics for lithium-ion battery packs based on a cell to pack method. ChinChin. J. Mech. Eng. *35*, 4.

36. Sui, X., He, S., Meng, J., Teodorescu, R., and Stroe, D.I. (2021). Fuzzy Entropy-Based State of Health Estimation for Li-Ion Batteries. IEEE Journal of Emerging and Selected Topics in Power Electronics *9*, 5125–5137.

37. Tian, J., Xiong, R., Shen, W., Lu, J., and Sun, F. (2022). Flexible battery state of health and state of charge estimation using partial charging data and deep learning. Energy Storage Mater. *51*, 372–381.

38. Che, Y., Stroe, D.I., Hu, X., and Teodorescu, R. (2023). Semi-supervised self-learning-based lifetime prediction for batteries. IEEE Trans. Ind. Inf. *19*, 6471–6481.

39. Wei, Z., Ruan, H., Li, Y., Li, J., Zhang, C., and He, H. (2022). Multistage State of Health Estimation of Lithium-Ion Battery with High Tolerance to Heavily Partial Charging. IEEE Trans. Power Electron. *37*, 7432–7442.

40. Liu, K., Peng, Q., Che, Y., Zheng, Y., Li, K., Teodorescu, R., Widanage, D., and Barai, A. (2023). Transfer learning for battery smarter state estimation and ageing prognostics : Recent progress , challenges , and prospects. Advances in Applied Energy *9*, 100117.

41. Ma, G., Xu, S., Yang, T., Du, Z., Zhu, L., Ding, H., and Yuan, Y. (2022). A Transfer Learning-Based Method for Personalized State of Health Estimation of Lithium-Ion Batteries. IEEE Trans. Neural Netw. Learn. Syst. *1*, 1–11.

42. Han, T., Wang, Z., and Meng, H. (2022). End-to-end capacity estimation of Lithium-ion batteries with an enhanced long short-term memory network considering domain adaptation. J. Power Sources *520*, 230823.

43. Lu, J., Xiong, R., Tian, J., Wang, C., Sun, F., and Tian, J. (2023). Deep learning to estimate battery state of health without additional degradation experiments. Nat. Commun. 1–13.

44. Li, S., He, H., Zhao, P., and Cheng, S. (2022). Health-Conscious vehicle battery state estimation based on deep transfer learning. Appl. Energy *316*, 119120.

45. Tan, Y., and Zhao, G. (2020). Transfer learning with long short-term memory network for state-of-health prediction of lithium-ion batteries. IEEE Trans. Ind. Electron. *67*, 8723–8731.

46. Shu, X., Shen, J., Li, G., Zhang, Y., Chen, Z., and Liu, Y. (2021). A Flexible State-of-Health Prediction Scheme for Lithium-Ion Battery Packs with Long Short-Term Memory Network and Transfer Learning. IEEE Transactions on Transportation Electrification *7*, 2238–2248.

47. Che, Y., Deng, Z., Lin, X., Hu, L., and Hu, X. (2021). Predictive Battery Health Management With Transfer Learning and Online Model Correction. IEEE Trans. Veh. Technol. *70*, 1269–1277.

48. Tang, X., Liu, K., Li, K., Widanage, W.D., Kendrick, E., and Gao, F. (2021). Recovering large-scale battery aging dataset with machine learning. Patterns *2*, 100302.

49. Sulzer, V., Mohtat, P., Aitio, A., Lee, S., Yeh, Y.T., Steinbacher, F., Khan, M.U., Lee, J.W., Siegel, J.B., Stefanopoulou, A.G., and Howey, D.A. (2021). The challenge and opportunity of battery lifetime prediction from field data. Joule *5*, 1934–1955.

50. Che, Y., Hu, X., and Teodorescu, R. (2023). Opportunities for battery aging mode diagnosis of renewable energy storage. Joule *7*, 1405–1407.

51. Che, Y., Zheng, Y., Sui, X., and Teodorescu, R. (2023). Boosting battery state of health estimation based on self-supervised learning. J. Energy Chem. *84*, 335–346.

52. Kirkpatrick, J., Pascanu, R., Rabinowitz, N., Veness, J., Desjardins, G., Rusu, A.A., Milan, K., Quan, J., Ramalho, T., Grabska-Barwinska, A., et al. (2017). Overcoming catastrophic forgetting in neural networks. Proc. Natl. Acad. Sci. USA *114*, 3521–3526.

53. Kemker, R., McClure, M., Abitino, A., Hayes, T.L., and Kanan, C. (2018). Measuring catastrophic forgetting in neural networks. In 32nd AAAI Conference on Artificial Intelligence, *2018*32nd AAAI Conference on Artificial Intelligence (AAAI), pp. 3390–3398.

54. Hadsell, R., Rao, D., Rusu, A.A., and Pascanu, R. (2020). Embracing Change: Continual Learning in Deep Neural Networks. Trends Cogn. Sci. *24*, 1028–1040.

55. Parisi, G.I., Kemker, R., Part, J.L., Kanan, C., and Wermter, S. (2019). Continual lifelong learning with neural networks: A review. Neural Netw. *113*, 54–71.

56. Du, M., Liu, N., and Hu, X. (2019). Techniques for interpretable machine learning. Commun. ACM *63*, 68–77.

57. Murdoch, W.J., Singh, C., Kumbier, K., Abbasi-Asl, R., and Yu, B. (2019). Definitions, methods, and applications in interpretable machine learning. Proc. Natl. Acad. Sci. USA *116*, 22071–22080.

58. Vlijmen, B.V., Asinger, P.A., Lam, V., Cui, X., Sun, S., Herring, P.K., Balaji, C., Geise, N., Deng, H.D., Thaman, H.L., et al. (2023). Interpretable Data-Driven Modeling Reveals Complexity of Battery Aging. Preprint at ChemRxiv.

59. Pozzato, G., Allam, A., Pulvirenti, L., Negoita, G.A., Paxton, W.A., and Onori, S. (2023). Analysis and key findings from real-world electric vehicle field data. Joule *7*, 2035–2053.

60. Deng, Z., Xu, L., Liu, H., Hu, X., Duan, Z., and Xu, Y. (2023). Prognostics of battery capacity based on charging data and data-driven methods for on-road vehicles. Appl. Energy *339*, 120954.

61. Wang, S., Miao, H., Li, J., and Cao, J. (2022). Spatio-Temporal Knowledge Transfer for Urban Crowd Flow Prediction via Deep Attentive Adaptation Networks. IEEE Trans. Intell. Transport. Syst. *23*, 4695–4705.

62. Ghifary, M., Bastiaan Kleijn, W., and Zhang, M. (2014). Domain adaptive neural networks for object recognition. Lect. Notes Comput. Sci. *8862*, 898–904.

63. Tzeng, E., Hoffman, J., Zhang, N., Saenko, K., and Darrell, T. (2014). Deep Domain Confusion: Maximizing for Domain Invariance. Preprint at arXiv.